Phonon Helicity Induced by Electronic Berry Curvature in Dirac Materials

Lun-Hui Hu, Jiabin Yu, Ion Garate, and Chao-Xing Liu

Phys. Rev. Lett. **127**, 125901 — Published 16 September 2021

DOI: 10.1103/PhysRevLett.127.125901

Phonon helicity induced by electronic Berry curvature in Dirac materials

Lun-Hui Hu,[1] Jiabin Yu,[2,1] Ion Garate,[3] and Chao-Xing Liu[1,*]

[1] *Department of Physics, the Pennsylvania State University, University Park, PA 16802*
[2] *Condensed Matter Theory Center, Department of Physics, University of Maryland, College Park, Maryland 20742, USA*
[3] *Département de Physique, Institut Quantique and Regroupement Québécois sur les Matériaux de Pointe, Université de Sherbrooke, Sherbrooke, Québec, Canada J1K 2R1*

In two-dimensional insulators with time-reversal (TR) symmetry, a nonzero local Berry curvature of low-energy massive Dirac fermions can give rise to nontrivial spin and charge responses, even though the integral of the Berry curvature over all occupied states is zero. In this work, we present a new effect induced by the electronic Berry curvature. By studying electron-phonon interactions in $BaMnSb_2$, a prototype two-dimensional Dirac material possessing two TR-related massive Dirac cones, we find that the nonzero local Berry curvature of electrons can induce a phonon angular momentum. The direction of this phonon angular momentum is locked to the phonon propagation direction, and thus we refer to it as "phonon helicity", in a way that is reminiscent of electron helicity in spin-orbit-coupled electronic systems. We discuss possible experimental probes of such phonon helicity.

Introduction - Berry phase and Berry curvature play a vital role in various branches of physics[1], owing to their deep connection to gauge field theories and differential geometry[2,3]. In condensed matter systems with broken TR symmetry, the integration of the electronic Berry curvature over all the occupied states in the first Brillouin zone underpins a number of Hall-related phenomena, including the quantum Hall and quantum anomalous Hall effect[4–7], (intrinsic) anomalous Hall effect[8] and orbital magnetic moments[9,10]. Similarly, the Berry phase and curvature of nonelectronic quasiparticles such as phonons and magnons lead to a thermal Hall effect in insulating crystals with broken TR[11–16]. In a TR invariant system, the integral of Berry curvature over all the occupied states vanishes. Nevertheless, nonvanishing Berry curvature can still appear locally in the Brillouin zone, inducing a variety of electronic phenomena, such as the spin[17] and valley Hall effects[18–20], nonlinear Hall effect[21–25], piezo-electromagnetic response[26–32] and quantized circular photo-galvanic effect in Weyl semimetals[33–36].

In certain two-dimensional (2D) insulators with TR symmetry, the low-energy electronic excitations are 2D massive Dirac fermions. In these systems, the gapped Dirac cones appear in pairs at two TR-related momenta (called two valleys below) with opposite local Berry curvatures due to TR symmetry. Although the total Hall conductivity vanishes, as proposed in Refs. [31] and [32], a nonzero Hall current can be induced by dynamical strain. Specifically, the dynamical strain plays the role of an artificial gauge field, dubbed "pseudo-gauge field" in literature[37]. One may wonder whether there are more ways (other than dynamical strain) to induce nonvanishing charge and spin response[17] for the local Berry curvature in TR invariant gapped systems. Furthermore, one may ask whether the electronic local Berry curvature can induce nontrivial behaviors in quasiparticles other than electrons.

In this work, we study the phonon dynamics in a prototype of 2D Dirac material, $BaMnSb_2$. By combining symmetry analysis and deformation potential theory, we find that the electron-phonon (e-ph) coupling in this material has the same form as the coupling between Dirac fermions and a U(1) gauge field, meaning that phonons can also act as pseudo-gauge fields and thereby induce nonvanishing Hall currents[31,32]. The electronic local Berry curvature can induce an out-of-plane phonon angular momentum (PAM), whose sign reverses for opposite in-plane phonon momenta. We refer to it as "phonon helicity", because it resembles the helical spin texture of spin-orbit-coupled bands in the momentum space for electronic systems. Specifically, the nonzero electronic local Berry curvature first introduces a self-energy correction to the phonon Green's function, which is an odd function of the phonon momentum $\mathbf{q}$, and then this self-energy correction makes the lattice vibration elliptical, eventually giving rise to nonzero PAM. This Berry-curvature contribution to phonon dynamics can be probed through measuring the total phonon angular momentum with a temperature gradient or through optical measurements of spatial dispersion of dielectric function.

Model Hamiltonian– We take $BaMnSb_2$ as a prototype model system. $BaMnSb_2$ is a layered material[38] with alternating Ba-Sb layers and Mn-Sb layers stacked along the (001) direction. Density-functional theory (DFT) calculations in Refs. [39] and [38] suggest that the electronic bands near the Fermi energy mainly come from the p-orbitals of the Sb atoms in the Ba-Sb layers, while the Mn-Sb layers serve as insulating barriers that prevent the tunneling of electrons along the (001) direction. Consequently, the bands near the Fermi energy are almost non-dispersive along the (001) direction, and thus $BaMnSb_2$ is a quasi-2D material. The unit cell in each Ba-Sb layer contains two Sb atoms, labeled as Sb_1 and Sb_2 in Fig. 1(a), both forming a square lattice. Distortion shifts Sb_2 atoms away from the center of the squares formed by Sb_1 atoms, resulting in a series of zig-zag chains. Due to the zig-zag distortion, the point group of $BaMnSb_2$ is C_{2v}, spanned by a two-fold rotation along

the x-axis (C_{2x}) and z-directional ($\sigma_v(xy)$) mirror planes. Magnetic moments in the Mn-Sb layers have little influence on the low-energy bands near the Fermi energy in the Ba-Sb layer, and thus the TR symmetry is taken into account.

We first describe the low-energy electronic properties. DFT calculations[38] indicate that the low-energy bands can be captured by two 2D massive Dirac cones at two momenta $K_\pm = (\pi/a, \pm k_{y_0})$, noted in Fig. 1(d). The energy band sequence around $K_\pm$ is schematically shown in Fig. 1(e), in which four low-energy bands at each momentum come from the two atomic orbitals ($p_{x,y}$ orbitals) and two spin states of Sb_1 atoms. The low-energy Hamiltonian is $\mathcal{H}_s = \int d^2k \Psi^\dagger_{s,\mathbf{k}} h_s(\mathbf{k}) \Psi_{s,\mathbf{k}}$ with

$$h_s(\mathbf{k}) = s v_0(k_y\tau_3 + k_x\tau_1) + s m_0 \tau_2, \tag{1}$$

where v_0 is the velocity of Dirac electrons and m_0 is the Dirac mass tuned by the zig-zag distortion. Here $s = \pm$ labels two valleys, and at each valley, the basis is labeled by $\Psi^\dagger_s(\mathbf{k}) = (c^\dagger_{s,p_x,\mathbf{k}}, c^\dagger_{s,p_y,\mathbf{k}})$, and $\tau_{i=0,1,2,3}$ are Pauli matrices for the orbital index. The spin-valley locking allows us to only consider electrons with one specific spin direction around each valley at low energies[38], as shown in Fig. 1(e). Within this low-energy subspace, $\sigma_v(xy)$ corresponds to an identity matrix and does not change the 2D momentum. Thus, we only consider C_{2x} and TR ($\mathcal{T}$) operations henceforth. The Hamiltonian (1) transforms as $C_{2x} h_s(k_x, k_y) C^{-1}_{2x} = h_{-s}(k_x, -k_y)$ and $\mathcal{T} h_s(\mathbf{k}) \mathcal{T}^{-1} = h_{-s}(-\mathbf{k})$, where the symmetry representations are $C_{2x} = \tau_3$ and $\mathcal{T} = \tau_0 \mathcal{K}$ ($\mathcal{K}$ stands for complex conjugation). Within one valley, we only have the combined symmetry $C_{2x}\mathcal{T} = \tau_3 \mathcal{K}$.

For the phonons, we focus on the in-plane vibrational modes, which are decoupled from the out-of-plane modes due to the opposite parities under $\sigma_v(xy)$. There are two Sb atoms in one unit cell and each atom can vibrate in the x or y direction. Thus, we have in total four phonon modes, two acoustic and two optical, which are classified according to the C_{2v} point group, as shown in table I of Sec. I.A in Supplemental Material (SM)[40]. Specifically, the lattice vibrations along the x and y directions are decoupled at $\mathbf{q} = 0$ due to the opposite signs under C_{2x}; the vibration patterns of these four modes are schematically shown in Fig. 1(b) and (c). The displacement vectors for these modes are labelled by $\vec{u}^a_{A_1}, \vec{u}^a_{B_1}, \vec{u}^o_{A_1}, \vec{u}^o_{B_1}$, where a/o are for acoustic and optical phonon modes and A_1, B_1 are the corresponding irreducible representations ($C_{2x}\vec{u}^{a/o}_{A_1} = \vec{u}^{a/o}_{A_1}$ and $C_{2x}\vec{u}^{a/o}_{B_1} = -\vec{u}^{a/o}_{B_1}$). These four phonon modes can also be obtained from the dynamical matrix for this system, as discussed in Sec. I.B of SM.

The e-ph coupling takes the general form

$$\mathcal{H}^\eta_{e-ph} = \sum_{\mathbf{k},\mathbf{q}} \sum_{\lambda,s,\alpha,\beta} \mathbf{g}^{\eta,\lambda,s}_{\alpha,\beta}(\mathbf{q}) Q_{\eta,\lambda,\mathbf{q}} c^\dagger_{s,\alpha,\mathbf{k}} c_{s,\beta,\mathbf{k}-\mathbf{q}}, \tag{2}$$

where $Q_{\eta,\lambda,\mathbf{q}} = (b_{\mathbf{q},\lambda} + b^\dagger_{-\mathbf{q},\lambda})/\sqrt{2M\omega_\lambda}$ labels the phonon displacement operator for the phonon mode $|\eta,\lambda\rangle$ (η for acoustic/optical and λ for A_1/B_1); M is the mass of Sb atoms; $b_{\mathbf{q},\lambda}$ is a bosonic operator that annihilates a phonon mode λ with momentum $\mathbf{q}$; α, β represent p-orbitals and $\mathbf{g}^{\eta,\lambda,s}_{\alpha,\beta}(\mathbf{q})$ is the element of the e-ph coupling vertex, which satisfies the Hermitian condition $\mathbf{g}^{\eta,\lambda,s}(\mathbf{q}) = [\mathbf{g}^{\eta,\lambda,s}(-\mathbf{q})]^\dagger$. The detailed form of $\mathbf{g}^{\eta,\lambda,s}$ can be derived from the deformation theory combined with the $\mathbf{k}\cdot\mathbf{p}$ theory, as shown in Secs. II and III of SM[40]. Here we only focus on long-wavelength optical phonons (dropping the index η below) and keep the spin-conserving intra-valley scattering process. Thus, we obtain

$$\mathbf{g}^{A_1,s} = g_0\tau_0 + s g_2 \tau_2 + g_3\tau_3;\ \mathbf{g}^{B_1,s} = g_1\tau_1, \tag{3}$$

to the lowest order in $\mathbf{q}$, where g_i's are real and material-dependent parameters[41,42]. The e-ph coupling vertex matrices satisfy the relations $C_{2x}\mathcal{T}\mathbf{g}^{A_1,s}\mathcal{T}^{-1}C^{-1}_{2x} = \mathbf{g}^{A_1,s}$ and $C_{2x}\mathcal{T}\mathbf{g}^{B_1,s}\mathcal{T}^{-1}C^{-1}_{2x} = -\mathbf{g}^{B_1,s}$. Comparing Eq. (3) with Eq. (1) (see Sec. II.C of SM[40]), one can see that g_0, g_1 and g_3 terms lead to a pseudo-gauge field

$$A^s_{pse,\mu} = (g_0 Q_{A_1}, s\tfrac{g_1}{v_0} Q_{B_1}, s\tfrac{g_3}{v_0} Q_{A_1})_\mu, \tag{4}$$

where $e = 1$ is assumed and $\mu = 0, 1, 2$. The g_2 term acts as a correction to Dirac mass. Taking into account both valleys, we note that $\frac{g_1}{v_0}Q_{B_1}$ and $\frac{g_3}{v_0}Q_{A_1}$ couple to electrons oppositely at two valleys, while the coupling between $g_0 Q_{A_1}$ and electrons is the same for the two valleys. Similar considerations apply to acoustic phonons as well (cf. Sec. III of SM[40]).

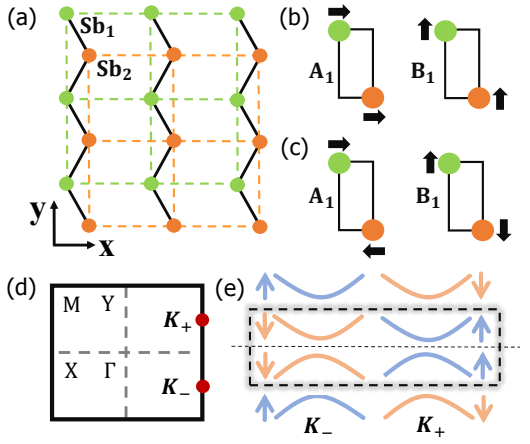

FIG. 1. (a) Lattice structure of $BaMnSb_2$. The green and orange dots represent two Sb atoms in each unit. Two acoustic phonons and two optical phonons are shown in (b) and (c), respectively. (d) First Brillouin zone. The two red dots label the location of two valleys $K_\pm$. (e) Low energy electron bands at Dirac cones $K_\pm$. The up/down-arrow represents spin polarization direction, and our model only focuses on the bands within the box with the dashed lines.

Phonon self-energy from electronic Berry curvature – Next, we study the optical phonon Green's function and the optical phonon spectrum renormalized by both electron-electron (e-e) and e-ph interactions.

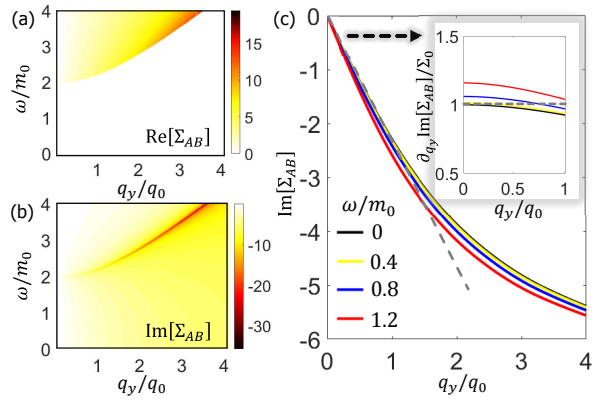

FIG. 2. The off-diagonal phonon self-energy Σ_{AB} induced by the electronic Berry curvature. We plot the real and imaginary parts of Σ_{AB} (in meV) as a function of ω/m_0 and q_y/q_0 in (a) and (b), respectively. (c) shows Im$[\Sigma_{AB}]$ as a function of q_y for the frequency values $\omega/m_0 = 0, 0.4, 0.8, 1.2$. The dashed line gives the pure contribution from the Berry curvature. The inset shows the partial derivative of Σ_{AB}. The parameter values are $m_0 = 25$ meV, $v_0 = 100$ nm·meV, $\omega_{A_1} = 20$ meV, $\omega_{B_1} = 30$ meV, and $g_0 = 80\sqrt{20}$ meV·nm^{-1}, $g_1 = 80\sqrt{30}$ meV·nm^{-1}. Also, $q_0 = m_0/v_0$ and $\Sigma_0 = g_0 g_1 \mathcal{A} N_3^+/(v_0 M\sqrt{\omega_A\omega_B})$.

The bare phonon Green's function is $D_0(q, i\omega_n) = \text{Diag}\{D_{A_1}, D_{B_1}\}$, where $D_\lambda = 2\omega_\lambda/((i\omega_n)^2 - \omega_\lambda^2)$ and ω_λ is the bare frequency for the λ mode. Here, $\omega_n = 2\pi n/\beta$ is the Matsubara frequency and $\beta = 1/k_B T$. Following standard formalism[42], the full phonon Green's function $D(\mathbf{q}, i\omega_n)$ can be obtained from $D^{-1}(\mathbf{q}, i\omega_n) = D_0^{-1}(\mathbf{q}, i\omega_n) - \Sigma(\mathbf{q}, i\omega_n)$, where the phonon self-energy $\Sigma = \Sigma^p + \Sigma^e$ contains both the correction from the bare e-ph interactions (Σ^p) and the additional correction due to the screened e-e Coulomb interaction (Σ^e). When the Fermi level μ is inside the bulk electronic gap ($|\mu| < 2|m_0|$) and when $|\omega| < 2|m_0|$, the Σ^e term only renormalizes the bare dielectric constant ϵ_0, the bare phonon energy ω_λ and the e-ph coupling strength g_i (see Sec. IV of the SM[40]). Hereafter, we only consider the contribution from the bare e-ph interaction (Σ^p) in Eq. (2), assuming that ω_λ and g_i^o have been renormalized by the e-e interaction. Thus, the superscript p is hereafter omitted.

The diagonal components of the phonon self-energies are then found to be $\Sigma_{AA} = (\Pi_{00} + \Pi_{33} + \Pi_{03} + \Pi_{30})/(2M\omega_A)$ and $\Sigma_{BB} = \Pi_{11}/(2M\omega_B)$, where

$$\Pi_{ij}(\mathbf{q}, i\omega_n) = \frac{g_i g_j}{\beta} \sum_{s,\mathbf{k},iq_m} \text{tr}[\tau_i G_s(\mathbf{k}, iq_m)\tau_j G_s(\mathbf{k}', i\omega_n')], \tag{5}$$

$\mathbf{k}' = \mathbf{k} + \mathbf{q}$, $i\omega_n' = i\omega_n + iq_m$, $q_m = (2m+1)\pi/\beta$, and $G_s(\mathbf{k}, iq_m) = [iq_m - h_s(\mathbf{k}) + \mu]^{-1}$ is the Matsubara Green's function for free electrons at valley K_s. The diagonal self-energies only provide corrections to the dispersion of the λ-phonon, and thus can be included by redefining $\omega_\lambda(\mathbf{q})$.

A more interesting physical effect emerges from the off-diagonal self-energy $\Sigma_{AB} = (\Pi_{01} + \Pi_{31})/(2M\sqrt{\omega_A\omega_B})$, where the contribution from the g_2 term has been neglected (see Sec. V of SM[40] for a detailed justification). Σ_{AB} hybridizes A and B phonons and has a deep connection to the Berry curvature of Dirac cones. To see that, we first consider $\omega = 0$ and treat $\mathbf{q}$ as a perturbation, so that $\Sigma_{AB}(\mathbf{q}, \omega = 0) = \Sigma_{AB}(0) + \mathbf{q}\cdot(\partial_{\mathbf{q}}\Sigma_{AB})_{\mathbf{q}=0} + \mathcal{O}(q^2)$. As shown in Sec. IV.C of SM[40], TR symmetry requires $\Sigma_{AB}(\mathbf{q}, \omega) = \Sigma_{AB}^*(-\mathbf{q}, \omega)$, while the C_{2x} symmetry leads to $\Sigma_{AB}(q_x, q_y, \omega) = -\Sigma_{AB}(q_x, -q_y, \omega)$. Combining these two symmetry constraints together with the perturbation expansion, we find $\Sigma_{AB}(\mathbf{q}, \omega = 0) \approx iq_y(\partial_{q_y}\text{Im}[\Sigma_{AB}])_{\mathbf{q}=0}$. We notice $\Sigma_{AB}(0) = 0$ since the A_1 and B_1 modes belong to different irreducible representations, but the q_y-dependent term is still allowed. Remarkably, a direct calculation gives

$$\left(\partial_{q_y}\text{Im}[\Sigma_{AB}(q_y, 0)]\right)_{q_y=0} = \frac{g_0 g_1 \mathcal{A}(N_3^+ - N_3^-)}{2v_0 M\sqrt{\omega_A\omega_B}}, \tag{6}$$

where $\mathcal{A}$ is the sample area and the coefficient $N_3^s = \frac{1}{6}\epsilon^{\alpha\beta\gamma}\text{tr}\int_{-\infty}^{\infty} d\omega' \int \frac{d^2k}{(2\pi)^2} G_s^{-1}\partial_{k_\alpha} G_s G_s^{-1}\partial_{k_\beta} G_s G_s^{-1}\partial_{k_\gamma} G_s$ is the Thouless-Kohmoto-Nightingale-den Nijs formula for the integral of the Berry curvature around the s-valley (i.e., the valley Chern number; see Sec. IV.D of SM[40]). TR requires $N_3^+ + N_3^- = 0$. Thus, to linear order in $\mathbf{q}$, $\Sigma_{AB}(\mathbf{q}) = ig_0 g_1 \mathcal{A} N_3^+ q_y/(v_0 M\sqrt{\omega_A\omega_B}) \triangleq iq_y\Sigma_0$, and the local Berry curvature around one valley enters into the off-diagonal phonon self-energy. This is a key result of the present work. Alternatively (see Sec. VI of SM[40]), Eq. (6) can be obtained from a Chern-Simons term that appears in the effective action for phonons after integrating out the electrons. Such derivation confirms that Σ_{AB} results from the valley Chern numbers.

The above analytical expression is derived in the limit $\omega \to 0$ and $\mathbf{q} \to 0$, while the λ-optical phonon has a finite frequency ω_λ. To see the finite frequency behavior of Σ_{AB}, we numerically evaluate it according to Eq. (5), and show the real and imaginary parts of Σ_{AB} in Fig. 2(a) and (b), respectively. When the frequency is larger than electron energy gap ($\omega > 2|m_0|$), the interband scattering of electrons from the conduction to valence bands can give rise to a large correction to the phonon self-energy. This is reflected by the red color lines for both Re$[\Sigma_{AB}]$ and Im$[\Sigma_{AB}]$ in Fig. 2(a) and (b), corresponding to the dynamical Kohn anomaly[43] occurring at $q = \sqrt{(\omega - m_0)^2 - m_0^2}$ for $\mu = 0$ (see Sec. VII of SM[40]). Below electron energy gap ($\omega < 2|m_0|$), Re$[\Sigma_{AB}]$ is exactly zero, while Im$[\Sigma_{AB}]$ is still non-zero. In Fig. 2(c), we plot Im$[\Sigma_{AB}]$ as a function of q_y for $\omega/m_0 = 0, 0.4, 0.8, 1.2$ separately, from which a linear-dependence on q_y appears in the long-wavelength limit. The pure Berry curvature contribution extracted from Eq. (6) is indicated by the gray dashed line, which shows a good coincidence with numerical results for a small q_y. The inset in Fig. 2(c) shows $(\partial_{q_y}\text{Im}[\Sigma_{AB}])/\Sigma_0$ at low q_y, and only a small derivation from unity is found for finite q_y and ω.

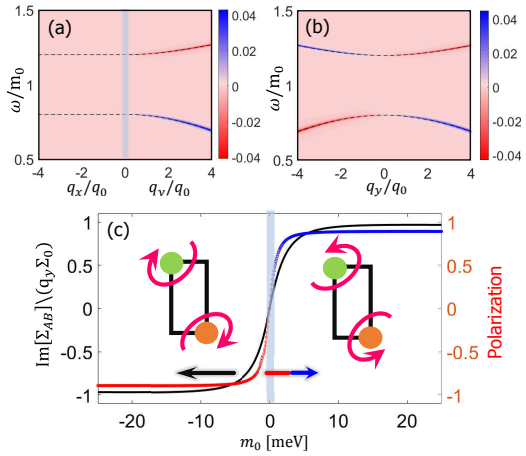

FIG. 3. (a) and (b) show the spectrum and angular momentum of optical phonons with $m_0 = 25$ meV. The phonon dispersions are labeled by black dashed lines, while the color represents $\mathcal{P}$ in Eq. (7). (c) shows $\mathrm{Im}[\Sigma_{AB}]$ (black line) and the phonon circular polarization (red and blue lines) as a function of m_0 with $q_y = m_0/2v_0$ and $\omega = 10$ meV. The phonon circular polarization has the same sign as $\mathcal{P}$. The inset is the schematics for the elliptical vibration of phonon modes. Parameters: $v_0 = 100$ meV·nm, $\omega_{A_1} = 20$ meV, $\omega_{B_1} = 30$ meV, $g_0 = 80\sqrt{20}$ meV·nm^{-1}, $g_1 = 80\sqrt{30}$ meV·nm^{-1}. Also, $q_0 = m_0/v_0$ and $\Sigma_0 = g_0 g_1 \mathcal{A} N_3^+/(v_0 M\sqrt{\omega_A \omega_B})$.

Therefore, our numerical simulations demonstrate that the Berry curvature contribution to the off-diagonal self-energy is dominant when the phonon frequency ω is well below electron energy gap. We notice that in a related material compound, $SrMnSb_2$, the optical phonon frequency has been measured to be ~ 15 meV[44], well below the expected electronic gap of ~ 50 meV.

Phonon helicity – Next, we explore the influence of Σ_{AB} in the phonon dynamics by studying the full phonon Green's function $D(\mathbf{q},\omega)$. The phonon dispersion can be directly extracted from the poles of $D(\mathbf{q},\omega)$, and is depicted by the black dashed lines in Fig. 3(a-b) for optical phonons. Since the A_1 and B_1 phonon modes describe lattice vibration along the x and y directions, respectively, and the off-diagonal term Σ_{AB} that couples these two modes is purely imaginary, we expect that Σ_{AB} can make phonon modes elliptically polarized at finite q_y, as schematically depicted in the inset of Fig. 3(c). To quantify this, we define the momentum-resolved PAM as

$$\mathcal{P}(\mathbf{q},\omega) = \mathrm{Tr}\left[\left(\hat{P}_+ - \hat{P}_-\right)\hat{A}(\mathbf{q},\omega)\right], \qquad (7)$$

where $\hat{A}(\mathbf{q},\omega) = i[D(\mathbf{q},\omega) - D^\dagger(\mathbf{q},\omega)]/(2\pi)$ is the phonon spectral function and the projection operators $\hat{P}_\pm = |\pm\rangle\langle\pm|$ project the phonon modes to the left and right circular polarized basis $|\pm\rangle = (\vec{u}_{o,A_1} \pm i\,\vec{u}_{o,B_1})/\sqrt{2}$. The total PAM discussed in literature[45–48] is the thermal average of $\mathcal{P}(\mathbf{q},\omega)$ over all the phonon modes. We highlight two features of $\mathcal{P}$: (1) $\mathcal{P}(\mathbf{q},\omega) = 0$ when $\mathbf{q}||\hat{\mathbf{x}}$ but $\mathcal{P}(\mathbf{q},\omega) \neq 0$ when $\mathbf{q}||\hat{\mathbf{y}}$ (see Fig. 3(a)); (2) $\mathcal{P}(q_y,\omega) = -\mathcal{P}(-q_y,\omega)$, as required by TR symmetry (see Fig. 3(b)). The latter feature suggests the helical nature of each phonon band and gives rise to phonon helicity. Both features can be understood from the symmetry property of Σ_{AB}: (1) Σ_{AB} vanishes along the q_x direction; (2) $\Sigma_{AB} \propto q_y$, so that its sign reverses under $q_y \to -q_y$.

More interestingly, since the local Berry curvature around one valley changes sign under a band inversion, we anticipate that the phonon helicity will also reverse its sign. To test this, we tune the Dirac mass m_0 in Eq. (1), and evaluate Σ_{AB} and $\mathcal{P}$ for the lower branch in Fig. 3(b) as a function of m_0 at the momentum $q_y = m_0/2v_0$ in Fig. 3(c). One can clearly see that both Σ_{AB} and $\mathcal{P}$ reverse signs across the phase transition point at $m_0 = 0$. Thus, we conclude that an electronic topological phase transition will leave its fingerprint on PAM $\mathcal{P}$.

We also notice that along the q_y direction, the B_1 mode is longitudinal while the A_1 mode is transverse. Therefore, a nonzero Σ_{AB} mixes the longitudinal and transverse modes of the in-plane phonons to form elliptical vibrational modes. The longitudinal-transverse mixing has been discussed previously in the context of the phonon Hall viscosity[49–51]. However, there is an essential difference: our system does not break TR while the phonon Hall viscosity breaks TR. Consequently, in Ref. [49], the PAM is an even function of $\mathbf{q}$, as reflected by the q^2-dependent coupling term between the longitudinal and transverse modes, while in our system, the PAM is an odd function of $\mathbf{q}$, thereby generating phonon helicity.

Discussion and Conclusion–. We have demonstrated that electronic Berry curvature in a 2D TR-invariant Dirac material can induce an off-diagonal self-energy correction to the optical phonon Green's function, giving rise to elliptical polarization of phonon modes. Our theory can also be directly applied to acoustic phonons. However, the e-ph coupling linearly depends on $\mathbf{q}$ for acoustic phonons, and thus the off-diagonal phonon self-energy has a q_y^3 dependence, as discussed in Sec. VI of SM[40].

Our study is qualitatively different from recent works investigating the influence of the chiral anomaly on sound velocity and attenuation in Weyl/Dirac semimetals[52–56]. For one thing, we focus on electrical insulators. Despite of several early works studying the Berry phase effect on phonon dynamics[14–16], the influence of electronic band topology on the PAM and helicity have not been mentioned before. Furthermore, although we take $BaMnSb_2$ as an example, the proposed mechanism for generating phonon helicity might be adapted to other Dirac materials. While a careful treatment is required to verify this for each material, possible candidates include HgTe/CdTe and InAs/GaSb quantum wells[57–60], $(LaO)_2(SbSe_2)_2$[61], boron nitride[62,63], 1T'-WTe_2[64–66], and others[67–70].

The Berry curvature contribution to phonon helicity can be detected in the following ways. Due to TR symmetry, the equilibrium phonon occupation number is symmetric under $q_y \to -q_y$; the total PAM is accordingly zero. However, away from equilibrium, a temperature gradient applied along the y axis breaks the $q_y \to -q_y$

symmetry and, combined with phonon helicity, leads to a nonzero total PAM. This mechanism is analogous to the Edelstein effect in electronic systems and has been discussed in Ref. [47]. For the optical phonon that can directly couple to light, the elliptical polarization will be reflected in the dielectric function and thus might be probed through optical measurements, as discussed in Sec. VIII of SM[40].

Acknowledgments–. We thank Zhen Bi, Shengxi Huang, Jainendra Jain, Ziqiang Mao, Yinming Shao, and Shuang Zhang for helpful discussions. C.-X. Liu and L.-H. Hu acknowledge the support of the Office of Naval Research (Grant No. N00014-18-1-2793) and Kaufman New Initiative research Grant No. KA2018-98553 of the Pittsburgh Foundation. I. Garate acknowledges financial support from the Canada First Research Excellence Fund (CFREF) and the Natural Sciences and Engineering Research Council of Canada (NSERC). J. Yu is supported by the Laboratory for Physical Sciences.

* cxl56@psu.edu

1 M. V. Berry, Proceedings of the Royal Society of London. A. Mathematical and Physical Sciences **392**, 45 (1984).
2 B. Simon, Phys. Rev. Lett. **51**, 2167 (1983).
3 D. Xiao, M.-C. Chang, and Q. Niu, Rev. Mod. Phys. **82**, 1959 (2010).
4 K. v. Klitzing, G. Dorda, and M. Pepper, Phys. Rev. Lett. **45**, 494 (1980).
5 D. J. Thouless, M. Kohmoto, M. P. Nightingale, and M. den Nijs, Phys. Rev. Lett. **49**, 405 (1982).
6 F. D. M. Haldane, Phys. Rev. Lett. **61**, 2015 (1988).
7 C.-Z. Chang, J. Zhang, X. Feng, J. Shen, Z. Zhang, M. Guo, K. Li, Y. Ou, P. Wei, L.-L. Wang, *et al.*, Science **340**, 167 (2013).
8 N. Nagaosa, J. Sinova, S. Onoda, A. H. MacDonald, and N. P. Ong, Rev. Mod. Phys. **82**, 1539 (2010).
9 D. Xiao, J. Shi, and Q. Niu, Phys. Rev. Lett. **95**, 137204 (2005).
10 D. Xiao, Y. Yao, Z. Fang, and Q. Niu, Phys. Rev. Lett. **97**, 026603 (2006).
11 X. Zhang, Y. Zhang, S. Okamoto, and D. Xiao, Phys. Rev. Lett. **123**, 167202 (2019).
12 R. Takahashi and N. Nagaosa, Phys. Rev. Lett. **117**, 217205 (2016).
13 S. Park and B.-J. Yang, Phys. Rev. B **99**, 174435 (2019).
14 J.-T. Lu, M. Brandbyge, and P. Hedegård, Nano letters **10**, 1657 (2010).
15 K. Sun, Z. Gao, and J.-S. Wang, Phys. Rev. B **102**, 134311 (2020).
16 C. A. Mead and D. G. Truhlar, The Journal of Chemical Physics **70**, 2284 (1979).
17 J. Sinova, S. O. Valenzuela, J. Wunderlich, C. H. Back, and T. Jungwirth, Rev. Mod. Phys. **87**, 1213 (2015).
18 D. Xiao, W. Yao, and Q. Niu, Phys. Rev. Lett. **99**, 236809 (2007).
19 D. Xiao, G.-B. Liu, W. Feng, X. Xu, and W. Yao, Phys. Rev. Lett. **108**, 196802 (2012).
20 K. F. Mak, K. L. McGill, J. Park, and P. L. McEuen, Science **344**, 1489 (2014).
21 I. Sodemann and L. Fu, Phys. Rev. Lett. **115**, 216806 (2015).
22 Y. Zhang, Y. Sun, and B. Yan, Phys. Rev. B **97**, 041101 (2018).
23 S.-Y. Xu, Q. Ma, H. Shen, V. Fatemi, S. Wu, T.-R. Chang, G. Chang, A. M. M. Valdivia, C.-K. Chan, Q. D. Gibson, *et al.*, Nature Physics **14**, 900 (2018).
24 Q. Ma, S.-Y. Xu, H. Shen, D. MacNeill, V. Fatemi, T.-R. Chang, A. M. M. Valdivia, S. Wu, Z. Du, C.-H. Hsu, *et al.*, Nature **565**, 337 (2019).
25 K. Kang, T. Li, E. Sohn, J. Shan, and K. F. Mak, Nature materials **18**, 324 (2019).
26 R. M. Martin, Phys. Rev. B **5**, 1607 (1972).
27 D. Vanderbilt, Journal of Physics and Chemistry of Solids **61**, 147 (2000).
28 A. Vaezi, N. Abedpour, R. Asgari, A. Cortijo, and M. A. H. Vozmediano, Phys. Rev. B **88**, 125406 (2013).
29 M. Droth, G. Burkard, and V. M. Pereira, Phys. Rev. B **94**, 075404 (2016).
30 H. Rostami, F. Guinea, M. Polini, and R. Roldán, npj 2D Materials and Applications **2**, 1 (2018).
31 J. Yu and C.-X. Liu, Nature communications **11**, 1 (2020).
32 J. Yu, B. J. Wieder, and C.-X. Liu, arXiv preprint arXiv:2008.10620 (2020).
33 F. de Juan, A. G. Grushin, T. Morimoto, and J. E. Moore, Nature communications **8**, 1 (2017).
34 Y. Zhang, H. Ishizuka, J. van den Brink, C. Felser, B. Yan, and N. Nagaosa, Phys. Rev. B **97**, 241118 (2018).
35 J. E. Moore, National Science Review **6**, 206 (2019).
36 D. Rees, K. Manna, B. Lu, T. Morimoto, H. Borrmann, C. Felser, J. Moore, D. H. Torchinsky, and J. Orenstein, Science advances **6**, eaba0509 (2020).
37 R. Ilan, A. G. Grushin, and D. I. Pikulin, Nature Reviews Physics **2**, 29 (2020).
38 J. Liu, J. Yu, J. Ning, H. Yi, L. Miao, L. Min, Y. Zhao, W. Ning, K. Lopez, Y. Zhu, *et al.*, Nature Communications **12**, 1 (2021).
39 M. A. Farhan, G. Lee, and J. H. Shim, Journal of Physics: Condensed Matter **26**, 042201 (2014).
40 See Supplemental Material at [URL] for details of long-wavelength in-plane phonon modes, electron-phonon interaction Hamiltonian for both optical phonons and acoustic phonons, Greens function for two coupled phonon modes, the additional self-energy correction due to the g_2^o e-ph coupling vertex, field-theoretic derivation for the off-diagonal coupling between phonons, phonon helicity for acoustic phonons, the dynamical Kohn anomaly, and the spatial dispersion of the dielectric function, which includes Refs. [38, 41–43, 71–79].
41 A. A. Abrikosov, L. P. Gorkov, and I. E. Dzyaloshinski, *Methods of quantum field theory in statistical physics* (Courier Corporation, 2012).
42 G. D. Mahan, *Many-particle physics*, Physics of Solids and Liquids (Springer Science & Business Media, 2013).
43 W.-K. Tse, B. Y.-K. Hu, and S. Das Sarma, Phys. Rev. Lett. **101**, 066401 (2008).
44 C. P. Weber, M. G. Masten, T. C. Ogloza, B. S. Berggren, M. K. L. Man, K. M. Dani, J. Liu, Z. Mao, D. D. Klug, A. A. Adeleke, and Y. Yao, Phys. Rev. B **98**, 155115

(2018).
[45] L. Zhang and Q. Niu, Phys. Rev. Lett. **112**, 085503 (2014).
[46] L. Zhang and Q. Niu, Phys. Rev. Lett. **115**, 115502 (2015).
[47] M. Hamada, E. Minamitani, M. Hirayama, and S. Murakami, Phys. Rev. Lett. **121**, 175301 (2018).
[48] D. M. Juraschek and N. A. Spaldin, Phys. Rev. Materials **3**, 064405 (2019).
[49] M. Barkeshli, S. B. Chung, and X.-L. Qi, Phys. Rev. B **85**, 245107 (2012).
[50] D. Liu and J. Shi, Phys. Rev. Lett. **119**, 075301 (2017).
[51] S. Heidari, A. Cortijo, and R. Asgari, Phys. Rev. B **100**, 165427 (2019).
[52] M. N. Chernodub and M. A. H. Vozmediano, Phys. Rev. Research **1**, 032040 (2019).
[53] F. Laliberté, F. Bélanger, N. L. Nair, J. G. Analytis, M.-E. Boulanger, M. Dion, L. Taillefer, and J. A. Quilliam, Phys. Rev. B **102**, 125104 (2020).
[54] S. Sengupta, M. N. Y. Lhachemi, and I. Garate, Phys. Rev. Lett. **125**, 146402 (2020).
[55] O. Antebi, D. A. Pesin, A. V. Andreev, and R. Ilan, Phys. Rev. B **103**, 214309 (2021).
[56] P. O. Sukhachov and L. I. Glazman, Phys. Rev. B **103**, 214310 (2021).
[57] B. A. Bernevig, T. L. Hughes, and S.-C. Zhang, science **314**, 1757 (2006).
[58] M. König, S. Wiedmann, C. Brüne, A. Roth, H. Buhmann, L. W. Molenkamp, X.-L. Qi, and S.-C. Zhang, Science **318**, 766 (2007).
[59] C. Liu, T. L. Hughes, X.-L. Qi, K. Wang, and S.-C. Zhang, Phys. Rev. Lett. **100**, 236601 (2008).
[60] I. Knez, R.-R. Du, and G. Sullivan, Phys. Rev. Lett. **107**, 136603 (2011).
[61] X.-Y. Dong, J.-F. Wang, R.-X. Zhang, W.-H. Duan, B.-F. Zhu, J. O. Sofo, and C.-X. Liu, Nature communications **6**, 1 (2015).
[62] J. Xue, J. Sanchez-Yamagishi, D. Bulmash, P. Jacquod, A. Deshpande, K. Watanabe, T. Taniguchi, P. Jarillo-Herrero, and B. J. LeRoy, Nature materials **10**, 282 (2011).
[63] M. Yankowitz, J. Xue, D. Cormode, J. D. Sanchez-Yamagishi, K. Watanabe, T. Taniguchi, P. Jarillo-Herrero, P. Jacquod, and B. J. LeRoy, Nature physics **8**, 382 (2012).
[64] S. Wu, V. Fatemi, Q. D. Gibson, K. Watanabe, T. Taniguchi, R. J. Cava, and P. Jarillo-Herrero, Science **359**, 76 (2018).
[65] Z. Fei, T. Palomaki, S. Wu, W. Zhao, X. Cai, B. Sun, P. Nguyen, J. Finney, X. Xu, and D. H. Cobden, Nature Physics **13**, 677 (2017).
[66] S. Tang, C. Zhang, D. Wong, Z. Pedramrazi, H.-Z. Tsai, C. Jia, B. Moritz, M. Claassen, H. Ryu, S. Kahn, *et al.*, Nature Physics **13**, 683 (2017).
[67] T. Wehling, A. M. Black-Schaffer, and A. V. Balatsky, Advances in Physics **63**, 1 (2014).
[68] J. Wang, S. Deng, Z. Liu, and Z. Liu, National Science Review **2**, 22 (2015).
[69] Y. Ren, Z. Qiao, and Q. Niu, Reports on Progress in Physics **79**, 066501 (2016).
[70] N. P. Armitage, E. J. Mele, and A. Vishwanath, Rev. Mod. Phys. **90**, 015001 (2018).
[71] G. D. M. S. Dresselhaus and A. Jorio, *Group theory: application to the physics of condensed matter* (Springer Science & Business Media, 2007).
[72] A. A. Maradudin and S. H. Vosko, Rev. Mod. Phys. **40**, 1 (1968).
[73] K. Saha, K. Légaré, and I. Garate, Phys. Rev. Lett. **115**, 176405 (2015).
[74] P. Rinkel, P. L. S. Lopes, and I. Garate, Phys. Rev. Lett. **119**, 107401 (2017).
[75] M. A. Vozmediano, M. Katsnelson, and F. Guinea, Physics Reports **496**, 109 (2010).
[76] E. H. Hwang and S. Das Sarma, Phys. Rev. B **75**, 205418 (2007).
[77] P. Pyatkovskiy, Journal of Physics: Condensed Matter **21**, 025506 (2008).
[78] A. Comtet, T. Jolicoeur, S. Ouvry, and F. David, *Aspects topologiques de la physique en basse dimension. Topological aspects of low dimensional systems*, Vol. 69 (Springer Science & Business Media, 2000).
[79] M. Srednicki, *Quantum field theory* (Cambridge University Press, 2007).